Research on Chemical Intermediates (2022) 48:1025–1044
https://doi.org/10.1007/s11164-021-04641-1

Microwave-assisted green synthesis of *Cyanthillium cinereum* mediated gold nanoparticles: Evaluation of its antibacterial, anticancer and catalytic degradation efficacy

Mamatha Susan Punnoose[1] · **Beena Mathew**[1]

Received: 13 September 2021 / Accepted: 15 December 2021 / Published online: 3 January 2022

Abstract

An eco-friendly and one-step microwave-assisted green synthesis of gold nanoparticles (AuNP) was developed using the aqueous leaf broth of *Cyanthillium cinereum* (CC) as the reducing and stabilizing agent. The progress of such bioconstituents stimulated experimental methods for the synthesis of gold particles in nanoregime is a key branch of nanotechnology due to its simple, sustainable and cost-effective nature. The prepared AuNP-CC particles were characterized using UV–vis., FT-IR, XRD, TEM, DLS and zeta potential analyses. The UV–vis. spectrum shows a surface plasmon resonance (SPR) at 548 nm. The FT-IR result proves the ability of CC extract to act as good capping and stabilizing agent for the nanoparticles. The high crystallinity of the AuNP-CC with face-centered cubic lattice phase was evident from XRD which is in accordance with bright circular rings of the obtained SAED patterns corresponding to (100), (200), (220) and (311) planes. The different morphologies and the estimated average nanoparticle size of 14.90 nm were analyzed using TEM. The negative zeta potential of − 19.2 mV suggested the stability of the formed nanoparticles. DLS measurement confirmed the diameter of nanoparticles to be in nanoscale. The catalytic potential of the AuNP-CC toward degradation of o-/p-nitro anilines was evaluated. The rapid catalytic reductions were monitored and found that they followed pseudo-first-order kinetic model. The linear dependence of the reaction rate constants with increase in catalytic dosage was also assessed. The cytotoxic activity of CC leaf extract and the gold nanoparticles were studied on human lung cancer cell line A549 using MTT assay. Studies shown that the cell viability (%) decreases with increasing sample dose, and nanoparticles have more toxic effect on the cancer cell than the pure CC extract. LC_{50} values were determined to be 110.19 ± 0.19 µg/mL and 87.92 ± 0.30 µg/mL for CC extract and AuNP-CC, respectively. The antibacterial activity of AuNP-CC was evaluated against four different human pathogenic bacteria. The excellent catalytic efficiency, cytotoxic and antibacterial activities of the green synthesized AuNP-CC are of great environmental benefits.

Extended author information available on the last page of the article

Keywords Green synthesis · Gold nanoparticles · *Cyanthillium cinereum* · Cytotoxic · Antibacterial · Catalytic degradation · o-/p-nitroanilines

Introduction

Over the past few years, noble metal nanoparticles have contributed much toward nanoscience and technology due to their eccentric size-dependent properties including electronic, optical, magnetic and thermal properties that dramatically differ from their bulk counterparts [1–3]. Among several noble metal nanoparticles, gold nanoparticles find immense applications in the fields of diagnosis, sensing, catalytic, drug delivery and imaging [4–6]. The high surface-to-volume ratio makes the gold nanoparticles as an attractive candidate toward catalytic applications [7].

The gold nanoparticles can be synthesized by various physical and chemical methods including sonochemical, photochemical, electrical, laser ablation and chemical reductions [8, 9]. Among them, chemical reduction methods were considered to be the best due to their control over the size and morphology of nanoparticles. Sodium borohydride, hydrazine and dimethyl formamide are the usually utilized reducing agents in the conventional reduction of gold salt to Au^0 [10]. As all these chemicals are highly reactive, toxic, harsh, expensive and often cause ecological injuries and have to be avoided from the synthetic pathways for nanoparticles [11]. The replacement of harsh chemicals by clean, nontoxic and environmental benign methods paves the way for the green synthesis of gold nanoparticles [12]. The green chemistry and bioprocess approach involve very negligible production of hazardous waste by-products and less consumption of energy than ordinary chemical synthetic means. Several biological systems such as plant extracts, bacteria, fungi, enzymes, natural polymers and gum can effectively reduce metal ions to their metal nanoparticles [13, 14].

Compared to chemical means of metal nanoparticle synthesis, biological methods are highly time consuming. The utilization of microwave energy is an alternative technique for the synthesis of metal nanoparticles. Microwave assistance provides numerous features such as shorter reaction time, higher reaction rate, better product yield and lesser utilization of energy as compared to traditional heating methods [15]. This mode of irradiation includes uniform heating of the reaction medium which results in the homogenous nucleation and formation of nanoparticles with narrower size distribution [16]. The drawback of longer reaction time requirement in the case of biological means of nanoparticle production is subdued by the action of unconventional microwave strategy, and it does not hinder the required green reaction conditions [11]. Recently, the green synthesis of gold nanoparticles using *Mussaenda glabrata* [17], *Synedrella nodiflora* [18] and *Myxopyrum serratulum* extract [19] with the aid of microwave energy is reported.

Cyanthillium cinereum are most commonly known as 'little ironweed' belongs to the family of *Asteraceae*, owing a wide range of geographical distribution. The plant possesses great medicinal value of traditional usage in many countries and also has recognition in *Ayurvedas*. *Cyanthillium cinereum* has therapeutic potentials against asthma, cancer, cholera, cough, diarrhea, fever, dysentery and

night-blindness [20]. Leaves are known to have analgesic, antipyretic and anti-inflammatory effects. Paste of stem and flowers is used to treat heal cuts, conjunctivitis, arthritis and rheumatism. Infusion of plant root is used as an antidote to scorpion sting and snake venom. Sesquiterpene lactone which have been isolated from this plant holds high antimalarial activity [21].

Aromatic nitro compounds are one among the most commonly used chemical groups in the manufacturing industries and are extremely hazardous when released into the environment. However, the reduced products of these nitroaromatics are extensively used in the preparations of polymers, rubber products, hair dyes and as intermediates for drugs in pharmaceutical industries [22]. Nowadays, the reduction of these types of anthrapogenic nitroaromatics by nanocatalyst in the presence of borohydride ions is widely used for the effectual removal of water contaminants. Over the recent years, the investigation of noble metallic nanoparticles for biomedical application has become a fast-growing area of research with great fascination. Distinct physicochemical properties of gold nanoparticles make them ideal for various biomedical applications such as anticancer activity. Green synthesis of gold nanoparticles utilizes medicinally important plant extracts like *Cyanthillium cinereum*, which may be retained on the nanoparticle surface and can act as novel agent in cancer therapy. Also, the green synthesized gold nanoparticles are receiving significant attention because of their biocompatibility and unique property to conjugate with proteins [23]. The gold nanoparticles minimize the risk of side effects and limit the damage to normal (noncancerous) cells [24]. The antibacterial efficiency of the gold nanoparticles was investigated by introducing the AuNP-CC particles into a cultural media of four different bacteria containing using standard agar well diffusion method.

The present study focused on the microwave-assisted synthesis of gold nanoparticles using the leaf extract of *Cyanthillium cinereum* and its characterization via UV–vis, FT-IR, XRD, TEM, EDX, DLS and zeta potential analyses. Antibacterial property of synthesized nanoparticles was examined for four various pathogenic bacteria. The in vitro cytotoxic activity of AuNP-CC was investigated through MTT assay against lung cancer cell line A549. Hence, catalytic performance of AuNP-CC toward the reduction of aromatic nitro compounds such as o-/p-nitroaniline in aqueous medium by using sodium borohydride as the reducing agent is also included in the current work.

Experimental

Materials

The hydrogen tetrachloro aurate (III) trihydrate, o-/p-nitroanilines and sodium borohydride were purchased from Sigma-Aldrich. All chemicals were used as such without further purifications. The aqueous solutions were prepared using double distilled water. Fresh leaves of *Cyanthillium cinereum* were collected and authenticated.

Methods

Preparation of *Cyanthillium cinereum* leaf extract

About twenty-five grams of the fresh collected leaves of *Cyanthillium cinereum* were weighed, washed thoroughly with distilled water, and slashed into tiny pieces. It was transferred into a 250 mL round bottom flask fitted with a water condenser and boiled with 100 mL double distilled water for an hour. It was cooled, filtered and stored at 4 °C for further studies.

Green synthesis of gold nanoparticles using *Cyanthillium cinereum* leaf extract (AuNP-CC)

10 mL of *Cyanthillium cinereum* leaf extract was well mixed with 90 mL auric trichloride (1 mM) solution in a 250 mL beaker. It was then subjected to microwave irradiation for about 5 min in a domestic microwave oven (Sharp R-219 T (W) at 2450 MHz and 800 W). Upon microwave heating, color of the solution mixture changed from pale yellow to violet confirming the formation of gold nanoparticles. It was further confirmed by monitoring the UV–vis. spectrum in the range of 200–800 nm.

Catalytic reduction studies

The catalytic reduction of o-/p-nitroanilines (1×10^{-4} M) involves the mixing of 2.5 mL of the organic pollutant with 0.5 mL freshly prepared $NaBH_4$ (0.6 M) solution and 0.25 mL AuNP-CC in a quartz cuvette of 1 cm path length. Variations in the absorbance of the characteristic peak of pollutants were recorded UV–vis. spectrophotometrically in the range of 200–800 nm at every one minute time.

In vitro cytotoxic studies using MTT assay

The cytotoxic effect of *Cyanthillium cinereum* (CC) leaf extract and AuNP-CC against A549 (Human Lung cancer) cells was determined using MTT assay. The cell lines were procured from National Centre for Cell Sciences (NCCS), Pune, India, and were maintained in Dulbecco's modified Eagles medium (DMEM) supplemented with 10% FBS, L-glutamine, sodium bicarbonate (Merck, Germany) and antibiotic solution containing: penicillin (100U/ml), streptomycin (100 µg/ml), and amphotericin B (2.5 µg/ml). Two days old confluent monolayer of cells was trypsinized and the cells were suspended in 10% growth medium, and 100 µl cell suspension (5×10^3 cells/well) was seeded in 96 well tissue culture plate. The cultured cell lines were kept at 37 °C in a humidified 5% CO_2 incubator (NBS Eppendorf, Germany). The viability of cells was evaluated by direct observation of cells by inverted phase contrast microscope and followed by MTT assay method.

Various amounts of the plant extract and gold nanoparticles (6.25, 12.5, 25, 50 and 100 µg/mL) were added to the grown cells and were incubated for 24 h. The untreated cells serve as the control. After incubation period, entire plates were observed using inverted phase contrast tissue culture microscope (Olympus CKX41 with Optika Pro5 CCD camera), and microscopic observation was recorded as images.

After 24 h of incubation period, the sample content in wells was removed and 30 µl of reconstituted MTT solution was added to all test and cell control wells, the plate was gently shaken well and then incubated for 4 h (at 37 °C in 5% CO_2 incubator). After the incubation period, the supernatant was removed and 100 µl of MTT solubilization solution (Dimethyl sulphoxide, DMSO, Sigma-Aldrich, the USA) was added and the wells were mixed gently by pipetting up and down in order to solubilize the formazan crystals. The absorbance values were measured by using microplate reader at a wavelength of 540 nm. The whole experiment is done in triplicate. The percentage of cell viability was calculated using,

$$\%\ \text{cell viability} = \frac{\text{Mean OD of Samples}}{\text{Mean OD of control}} \times 100$$

where 'OD' stands for optical density. The LC_{50} values were calculated using ED50 PLUS V1.0 software, and mean ± standard deviation was also identified.

Antibacterial studies

The potential of synthesized gold nanoparticles as antibacterial antifungal agents was accessed by using the agar well diffusion method. Petri plates containing 20 ml Muller Hinton agar medium were seeded with bacterial culture of *Escherichia coli*, *Pseudomonas aeruginosa*, *Streptococcus mutans* and *Staphylococcus aureus*. Wells of approximately 10 mm were bored using a well cutter, and 100µL of the samples were added. The plates were then incubated at 37 °C for 24 h. The antibacterial activity was assayed by measuring the diameter (in mm) of the inhibition zone formed around the well, and distilled water was used as the control.

Characterization

The biofabricated AuNP-CC particles were characterized using the following analyzing techniques. The UV–vis. spectra were recorded using Shimadzu UV-2450 spectrophotometer. FT-IR spectra were obtained from PerkinElmer-400 FT-IR spectrometer. XRD diffractions were measured using Bruker AXS D8 Advance X-ray Diffractometer. High-resolution transmission electron microscopic (HR-TEM) images were recorded by JEOL JEM-2100 microscope. Particle size and zeta potential measurements were carried out using Horiba SZ-100 Scientific nanoparticle analyzer.

Results and discussion

UV–vis. analysis

Within a one minute of microwave irradiation, the pale-colored solution mixture of CC extract and $HAuCl_4$ (1 mM) turned violet. The color change is associated with microwave heating and appearance of a characteristic surface plasmon resonance (SPR) peak at 548 nm indicates the complete reduction of Au^{3+} in $HAuCl_4$ to Au^0. The various phytochemicals present in the CC extract are responsible for this reduction. The UV–vis. spectrum of AuNP-CC is depicted in Fig. 1. The CC extract did not show any obvious peak in the visible region of the spectrum.

Compositional ratio between CC extract and $HAuCl_4$ solution, microwave irradiation power level and heating time were optimized for the synthesis of AuNP-CC. Figure 2a shows the different compositional trials between CC extract and gold salt solution for the green synthesis of AuNP-CC. In 1:3 ratio, no characteristic peak for the formation of nanoparticles occurred. The origin of absorption bands for 1:5 and 1:7 ratios with much less intensity indicates the commencement of the formation of nanoparticles. While 1:9 composition exhibited a sharp resonance peak at 548 nm which infer the monodispersive nature of the formed AuNP-CC particles. Hence, 1:9 ratio was preferred rather than other ratios for further studies.

Influence of microwave power level on the AuNP-CC synthesis using 1:9 composition was studied by changing the power from 200 to 800 W, by sustaining the time for microwave irradiation a constant. The intensity of resonance band increased with irradiation power level and reached a maximum at 800 W. With the increase in power level, absorption of energy by the solution mixture increases which results in the faster reduction of Au^{3+} ions. The absorbance bands obtained at the various power levels show that the one corresponding to 800 W was the most intense and sharp (Fig. 2b). Thus, the optimum power level of microwave irradiation was fixed at 800 W.

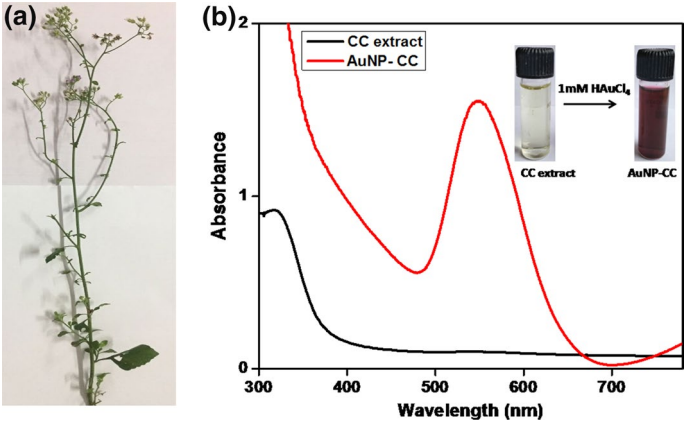

Fig. 1 **a** Photograph of *Cyanthillium cinereum* and **b** UV–vis. spectra of CC extract and AuNP-CC

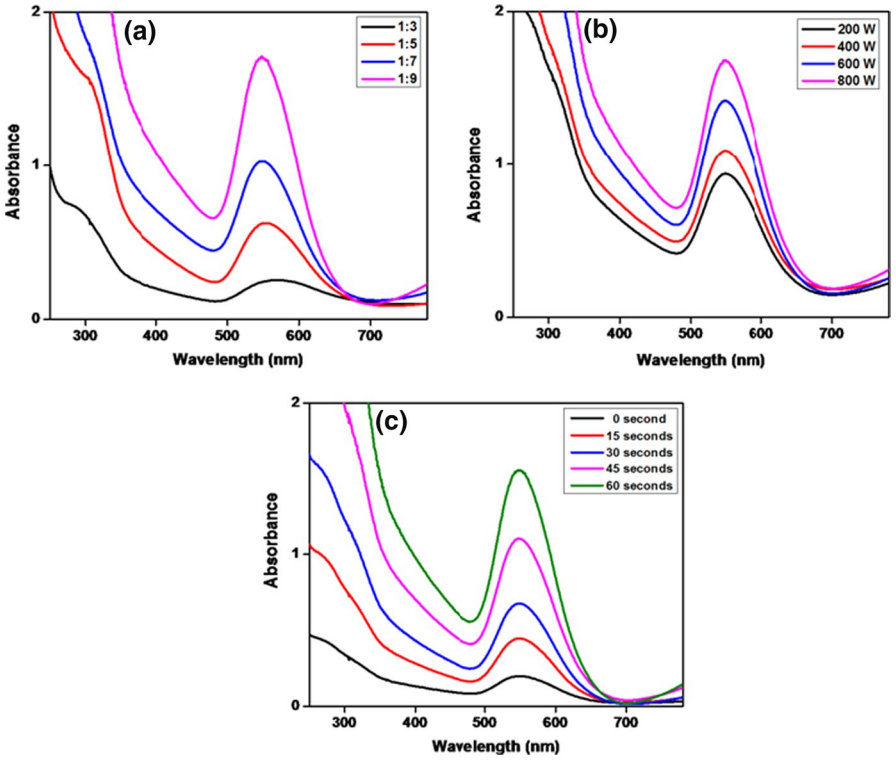

Fig. 2 UV–vis. spectra showing the influence of **a** compositional ratio between $HAuCl_4$ and CC extract, **b** microwave power level, and **c** microwave irradiation time for the formation of AuNP-CC

The effect of irradiation time on the synthesis of AuNP-CC was checked by UV–vis. spectrum in every 15 s of microwave heating. No characteristic SPR band was obtained at the initial stages of the irradiation. After 15 s of the irradiation, a SPR band appeared around 548 nm and its absorbance value increased with irradiation time and reached a maximum at 60 s (Fig. 2c). Even after 1 min of microwave irradiation, no significant change in the absorbance and position of the obtained peak was noted which indicates that nanoparticle formation was devoid of agglomeration [23].

FT-IR analysis

FT-IR spectrum reveals the involvement of the plant extract in the reduction of nanoparticles. The FT-IR spectra of CC extract and AgNP-CC are depicted in Fig. 3. The bands at 3259 and 1027 cm^{--1} correspond to the O–H and C-O stretching vibrations of phenolic groups present in the leaf extract. Bands at 2926 and 1573 cm^{-1} are characteristic of aliphatic C-H and aromatic C=C stretching vibrations, respectively. The band at 1381 cm^{-1} unveiled the bending vibrations of O–H

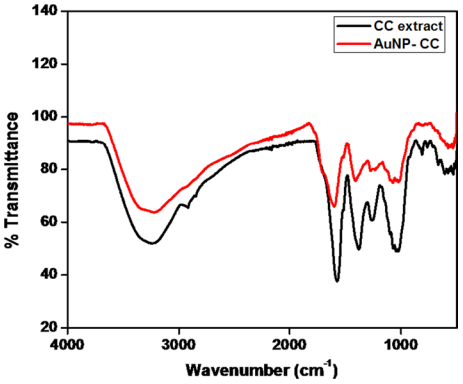

Fig. 3 FT-IR spectra of **a** *Cyanthillium cinereum* extract, and **b** AuNP-CC

[25]. A characteristic band of aromatic ring is observed at 824 cm^{-1}. Although the FT-IR spectra of CC extract and AgNP-CC appear to be alike, various bands of AgNP-CC are less intense than the CC extract. Compared to the spectrum of CC extract, AgNP-CC shows slight shift in their various band positions, which suggest the vital role of CC extract in the reduction and stabilization of the formed gold nanoparticles.

XRD analysis

The XRD spectrum clearly demonstrates the crystalline nature of prepared AuNP-CC as shown in Fig. 4. The four distinct peaks at two theta values of 38.04^0, 44.14^0, $64.47^0$and 77.57^0correspond to the reflection from (111), (200), (220) and (311) planes of the face-centered cubic lattice structure, respectively [26]. Out of the four diffraction patterns, the one corresponding to the (111) plane is the most intense which indicates that majority of the AuNP-CC nanoparticles are preferably oriented along this plane. These data are in accordance with JCPDS file no. 04–0784. The average crystalline size of the AuNP-CC was calculated using Debye–Scherrer equation, $D = K\lambda/\beta\cos\theta$, where '$D$' is the particle size, K is the Scherrer constant with a

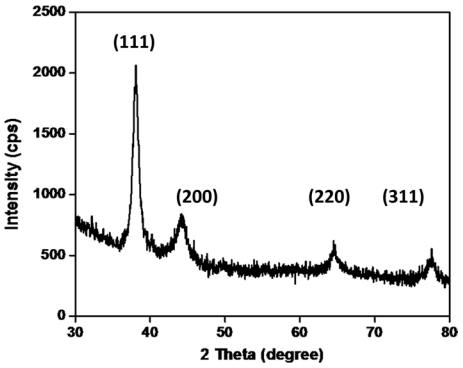

Fig. 4 XRD pattern of AuNP-CC

value of 0.9, 'λ' is the wavelength of X-ray source (0.1541 nm), 'β' is the full width at half maximum, and 'θ' is the diffraction angle that corresponds to lattice plane (111). From the Debye–Scherrer equation, the average crystallite size of AuNP-CC was found to be about 11.17 nm.

TEM and EDX analysis

The size and shape of the formed AuNP-CC nanoparticles were determined from TEM analysis. The TEM images at different magnifications show various shapes acquired by the gold nanoparticles such as spherical, triangular, truncated triangular and hexagonal (Fig. 5a and b). The size of nanoparticles varies between 8 and 24 nm with an average particle size of 14.90 nm, which is evident from the histogram of particle diameter distribution (Fig. 5c. Selected area electron diffraction (SAED) patterns show bright circular fringes corresponding to (111), (200), (220) and (311) planes which are in accordance with the obtained XRD results (Fig. 5d). These confirm the crystallinity of the AuNP- nanoparticles. The EDX spectrum shows the presence of gold signals (Fig. 5e). The signals of copper are from the copper grid used for the sample preparation.

DLS and zeta potential measurements

The typical size and particle size distribution of the synthesized AuNP-CC was obtained from DLS analysis. The average hydrodynamic diameter of the

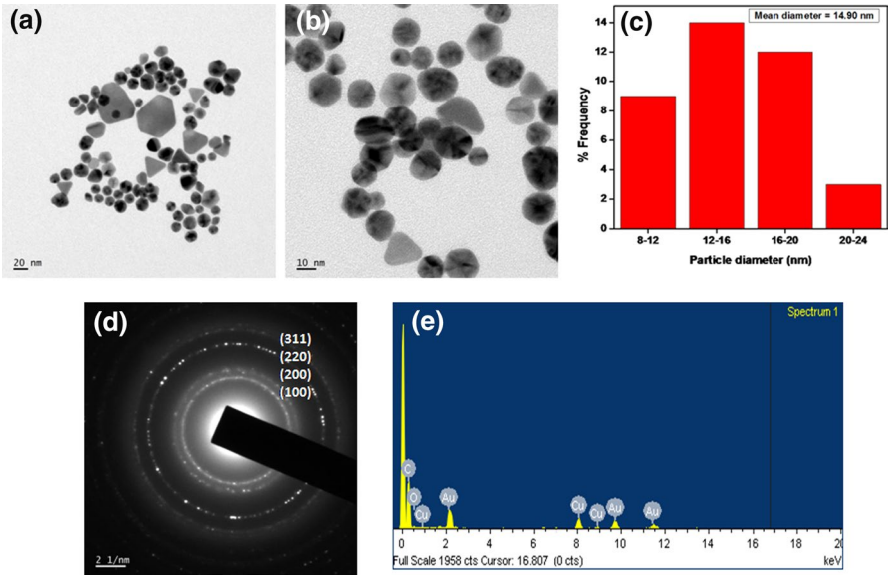

Fig. 5 **a** and **b** TEM images of AuNP-CC at different magnifications, **c** particle size histogram, **d** SAED pattern, and **e** EDX spectrum of AuNP-CC

monodispersed nanoparticle suspension was found to be 140.3 nm which is much greater than their TEM results. The average diameter in DLS is measured by means of dynamic light scattered from the core nanoparticles and the cloud of phytochemical constituents formed from the plant extract around the gold nanocore. While the diameter of individual particles is usually determined by TEM analysis. The zeta potential value of − 19.2 mV confirms the stability of the formed AuNP- nanoparticles. The negative value indicates the negative charge developed over the surface of nanoparticles. The details of DLS and zeta potential measurements of AuNP-CC are depicted in Fig. 6.

Catalytic reduction of environmental pollutants

In order to study the catalytic action of the green synthesized AuNP-CC, we have selected the reduction of o-/p-nitroanilines to their corresponding aminoarenes. These reductions were visually identified by the discoloration of the yellow color of nitroanilines, and the progress of the reaction was noted at regular intervals of one minute using UV–vis. spectroscopic analysis. Among the various genotoxic and environmental pollutants, nitroanilines were considered to be the most toxic due to their potential mutagenic and carcinogenic effects. Hence, release of these nitroaromatics into the environment prior to their reduction is often deleterious.

Nitroaromatic compounds are the main intermediates in the synthesis of azo dyes, pesticides, rubber products, fuel additives, antiseptic agents, polymers and pharmaceuticals [27]. The enhancement in the stability of nitro anilines provided by the presence of nitro group in the aromatic ring makes them highly resistant to conventional bio-chemical oxidation degradation processes [28]. Thus, the purification of wastewater carrying nitro anilines is quite difficult. The present work reports the efficient catalytic activity of AuNP-CC in the degradation of o-/p-nitroanilines by sodium borohydride.

In the UV–vis. spectrum, the aqueous solution of ortho- and para-nitroaniline exhibited characteristic absorption bands at 412 and 380 nm, respectively [29]. The reduction of aqueous o-/p-nitroaniline by $NaBH_4$ is shown in Fig. 7a and b. During the reaction, absorbance of the characteristic peaks remained almost intact, which indicated that the uncatalyzed reductions cannot be processed due to the high kinetic

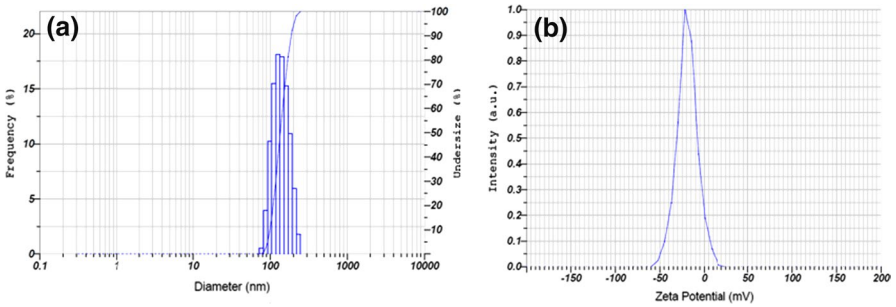

Fig. 6 **a** DLS measurement of AuNP-CC **b** zeta potential measurement of AuNP-CC

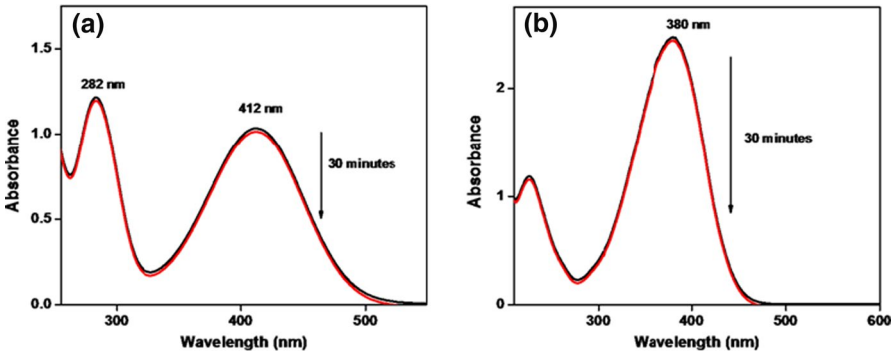

Fig. 7 UV–vis. spectra showing the reduction of **a** o-nitroaniline, and **a** p-nitroaniline in the presence of $NaBH_4$ alone

barrier though they are thermally favorable. Addition of AuNP-CC catalyst into the nitroaniline solution overcomes this kinetic barrier and facilitates the transfer of electrons from borohydride ions to nitroaniline acceptor moieties [30]. The complete reduction of o-/p-nitroanilines into their corresponding aromatic amino compounds is associated with a color change from yellow to colorless.

The progress in the catalytic reduction of o-nitroaniline in aqueous medium by AuNP-CC/ $NaBH_4$ was monitored with UV–vis. Spectroscopy by the alterations in peak absorbance at 412 and 282 nm as a function of time. The addition of gold nanocatalyst triggered the effectual reduction which is evident from the abrupt decrease in absorbance of peak maximum. By the lapse of time, reduction of the observed peak at 412 nm completed within a few minutes of the reaction. The analogous red shift of diminishing peak at 282 to 290 nm indicated the rapid conversion of o-nitroaniline to o-phenylene diamine (Fig. 8) [31].

The absorbance of peak at 380 nm decreased during the catalytic reduction of p-nitroaniline and two new peaks appeared simultaneously around 235 and 305 nm which are characteristic of p-phenylene diamine [32]. Time-dependent variations of p-nitroaniline at their characteristic absorbance at 380 nm upon the addition of various concentrations of AuNP-CC catalyst are shown in Fig. 9. These rapid reductions were attained within a few minutes. The very small particle size and available large surface area of the nanocatalyst furnish enormous number of available binding sites on its surface leading to the enhanced rate of catalytic reduction [33]. The product p-phenylene diamine formed by the hydrogenation of p-nitroaniline is the chief intermediate in the synthesis of various hair dyes, polymers and rubber products [34].

Kinetics of the hydrogenation reaction

Kong et al. [35] proposed that the hydrogenation of both o-/p-nitroanilines to the corresponding diamines by $NaBH_4$ was rather slow in the absence of a catalyst due to the substantial variations between the redox potentials of these pollutants and $NaBH_4$. Hence, these reactions are kinetically forbidden though thermally

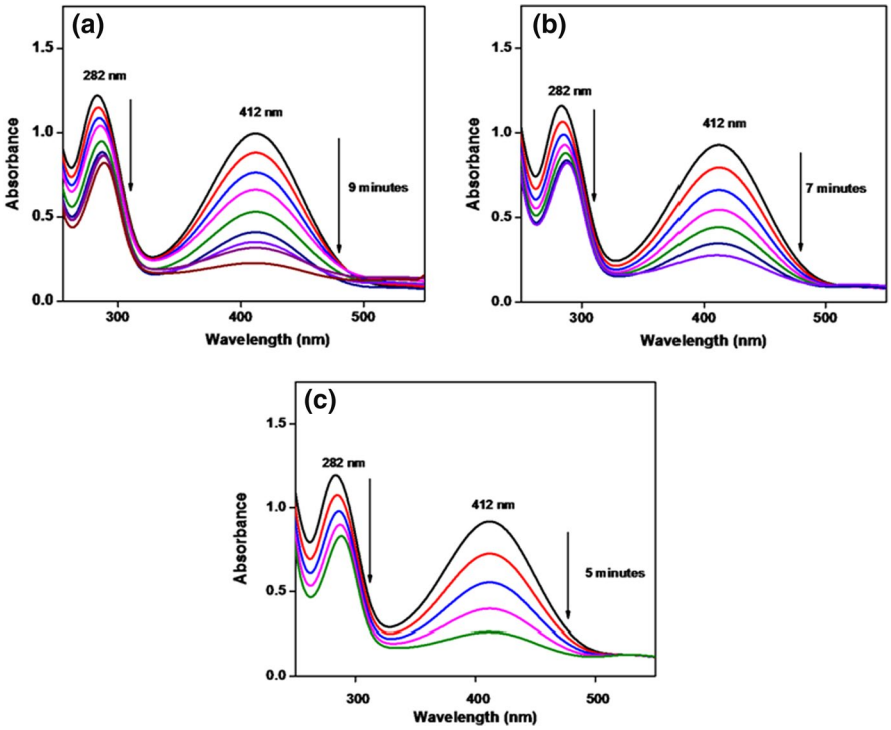

Fig. 8 UV–vis. spectra showing the reduction of o-nitroaniline by $NaBH_4$ in the presence of **a** 0.02 mg/mL, **b** 0.03 mg/mL and **c** 0.04 mg/mL AuNP-CC nanocatalyst

allowed [36]. The intermediate redox potential and large surface area of the nanocatalyst facilitate the electron transfer between the donor borohydride ions and the acceptor pollutant moieties upon adsorption of reactants onto the catalyst nanosurface [25]. The phytoconstituents surrounding the nanoparticles aid in the adsorption process by means of electrostatic forces of attraction between the donor–acceptor moieties. The borohydride ions eject electrons to the nanocatalyst surface, from which the acceptor o-/p-nitroanilines gain electrons and get reduced [37]. Thus, the presence of nanocatalyst makes a kinetically forbidden reaction an allowed one. Figure 10 represents the hydrogenation scheme for o-/p-nitroanilines by AuNP-CC/$NaBH_4$. The effect of catalytic concentration on both hydrogenation processes was evaluated by varying the catalyst dose, keeping all other parameters fixed.

Kinetics of both hydrogenations were spectrophotometrically monitored by tracing the variations of absorbance peaks at 412 and 380 nm, respectively, for ortho- and para-nitroanilines (Fig. 11). As the concentration of $NaBH_4$ used greatly exceeds that of the pollutants, its concentration practically remained to be a constant during entire course of reduction. Hence, the reactions followed pseudo-first-order kinetics with respect to each of the pollutants used. The rate

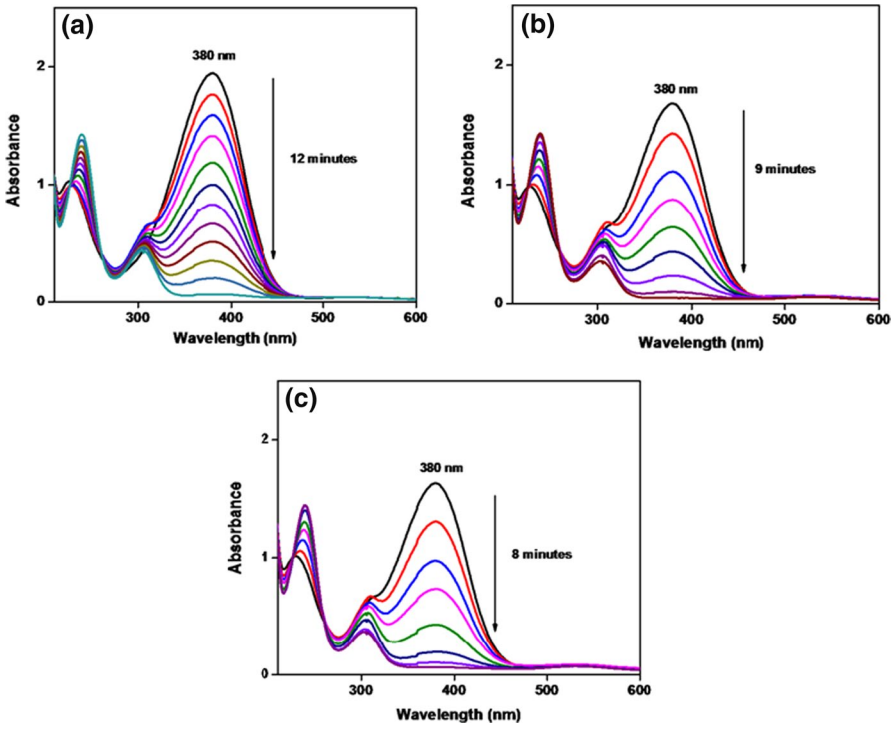

Fig. 9 UV–vis. spectra of the reduction of p-nitroaniline by $NaBH_4$ in the presence of **a** 0.02 mg/mL, **b** 0.03 mg/mL and **c** 0.04 mg/mL AuNP-CC nanocatalyst

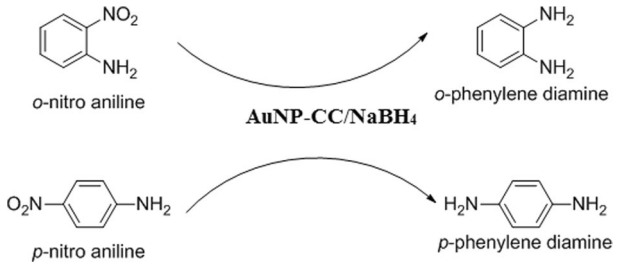

Fig. 10 Schematic representation of reduction of o-/p-nitroanilines

equation can be written as $k = 1/t \ln [A_0]/[A]$, where k stands for first-order reaction constant, $[A_0]$ for the initial concentration of the pollutants and [A] for their concentrations at t time. The ln[A] values obtained from the absorbance graph of the pollutants versus their corresponding hydrogenation time give a linear

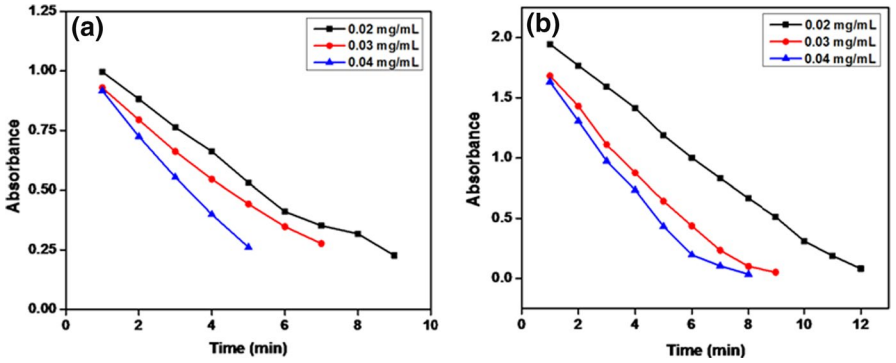

Fig. 11 Absorbance versus time plot for the reductions of **a** o-nitroaniline and **b** p-nitroaniline

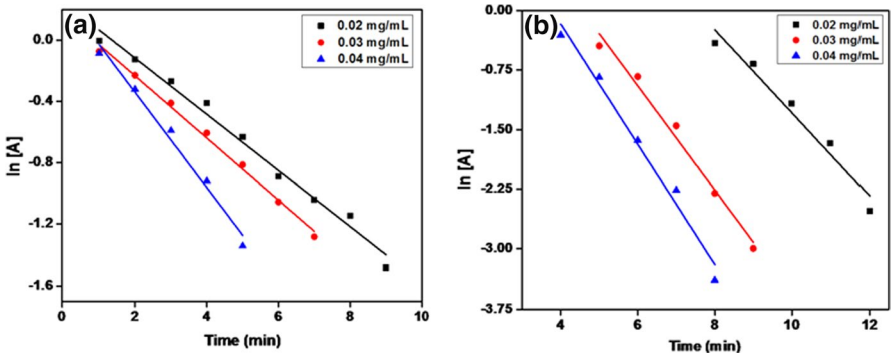

Fig. 12 Plot of ln [A] against time for the reductions of **a** o-nitroaniline **b** p-nitroaniline

Table 1 Catalytic activity of AuNP-CC in the reduction of o-nitroaniline

Concentration of AuNP ($mgmL^{-1}$)	Time (min)	Rate constant (k) (min^{-1})	Correlation coefficient (R^2)
0.02	9	0.1835	0.9585
0.03	7	0.2032	0.9940
0.04	5	0.3115	0.9808

plot (Fig. 12). Using the slopes of these linear plots, rate constants were easily calculated.

From Table 1 and Table 2, it is clear that the rate of the reduction increased with nanocatalyst dose with good correlation coefficients. The calculated rate constants are superior to the other reported green gold nanoparticles (Table 3). Figure 13a and b clearly indicates the linear relation between the reaction constant (k) and catalytic dosage of AuNP-CC.

Table 2 Catalytic activity of AuNP-CC in the reduction of p-nitroaniline

Concentration of AuNP ($mgmL^{-1}$)	Time (min)	Rate constant (k) (min^{-1})	Correlation coefficient (R^2)
0.02	12	0.5235	0.9502
0.03	9	0.6572	0.9793
0.04	8	0.7571	0.9784

Table 3 Comparison of catalytic reduction of o-/p-nitroanilines by AuNP-CC with reported green synthesized gold nanoparticles

Nitroaromatics	Gold nanoparticles	Rate constant (min^{-1})	References
	AuNP- *Delonix regia*	0.0319	[25]
o-nitroaniline	AuNP- *Litchi chinensis*	0.0618	[37]
	AuNP- *Indigofera tinctoria*	0.0673	[38]
	AuNP- *Staphylococcus warneri*	0.2510	[39]
	AuNP- *Cyanthillium cinereum*	0.3115	This work
p-nitroaniline	AuNP- *Sapindus mukorossi*	0.0450	[40]
	AuNP- *Pycnoporus sanguineus*	0.0650	[41]
	AuNP- *Indigofera tinctoria*	0.0824	[38]
	AuNP- *Litchi chinensis*	0.1456	[37]
	AuNP-*Citrus aurantifolia*	0.3313	[42]
	AuNP- *Cyanthillium cinereum*	0.7571	This work

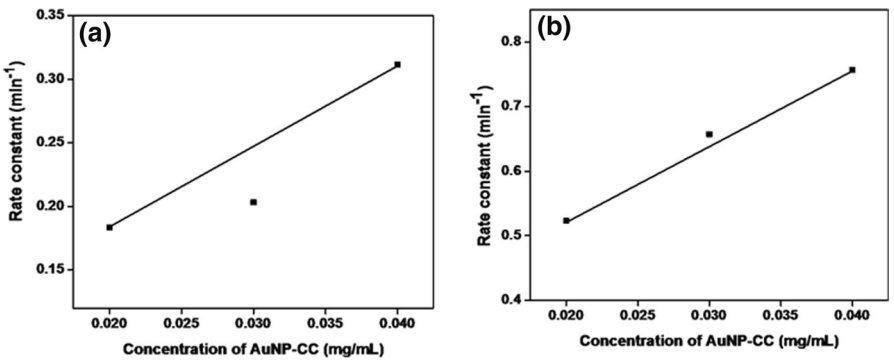

Fig. 13 Plots of rate constant (k) versus concentration of AuNP-CC for the reduction of **a** o-nitroaniline, and **b** p-nitroaniline

Cytotoxic studies

The cytotoxic effect of aqueous CC leaf extract and AuNP-CC was investigated on human lung cancer cell line, A549 using MTT assay. Morphological changes like shrinking of the cells induced by the CC extract and AuNP-CC are represented by

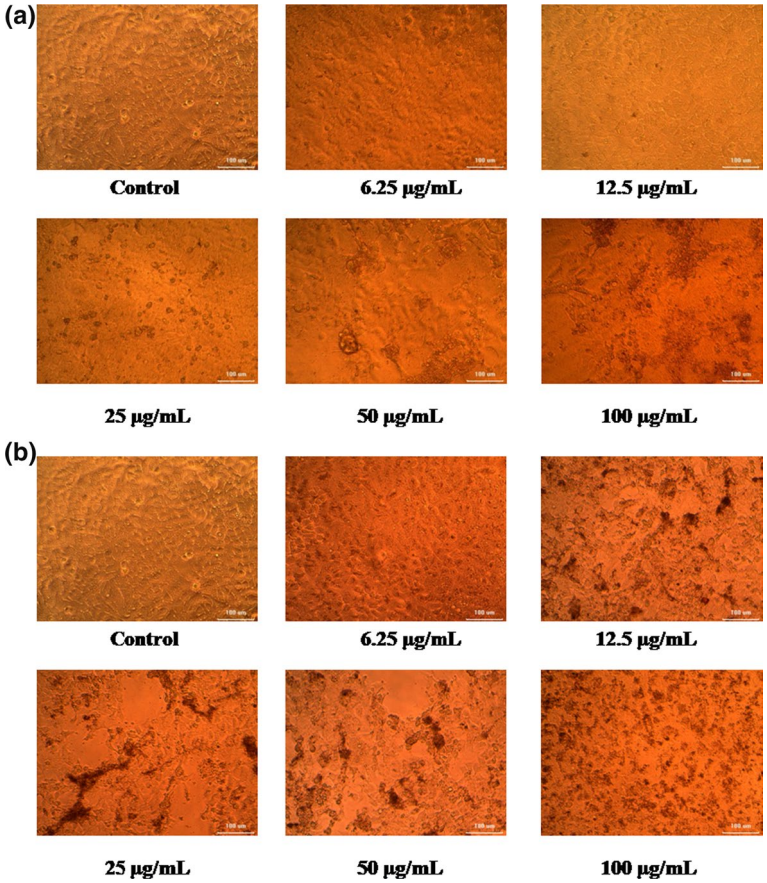

Fig. 14 Morphological changes induced on treated A549 cancer cell by **a** aqueous CC extract, and **b** AuNP-CC

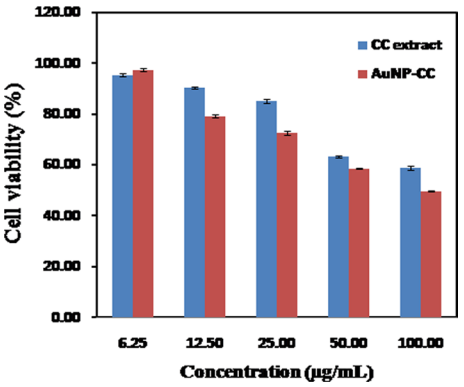

Fig. 15 The cell viability (%) of CC extract and AuNP-CC toward A549 cancer cell. Values are represented as the mean ± SD ($n = 3$)

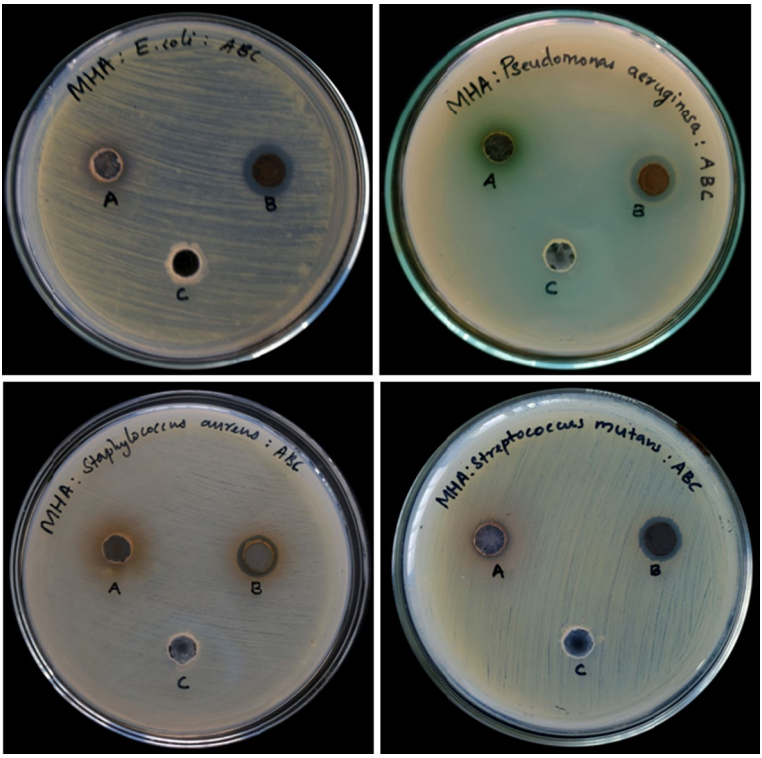

Fig. 16 Illustration of the antibacterial activity of AuNP-CC against *E. coli, P. aeruginosa*, *S. aureus* and *S. mutans* using agar well diffusion method. [A: CC extract, B: AuNP-CC and C: control]

Fig. 14a and b, respectively. Figure 15 shows the cell viability (%) on treatment with various concentrations of CC extract and AuNP-CC indicates that the viability of cells decreased with increase in concentration of the samples. The LC_{50} values were calculated using ED50 PLUS V1.0 software and were determined to be 110.19 ± 0.19 and 87.92 ± 0.30 µg/mL for leaf extract and AuNP-CC, respectively. Thus, it is clear that the required concentration to inhibit 50% lung cancer cell line (A549) is low for AuNP-CC than the CC extract. The antiproliferative activity exhibited by AuNP-CC may be due to the synergetic effect from both nano-sized gold and the bioactive phytoconstituents attached on the nanosurface [45].

Antibacterial studies

Antibacterial property of the synthesized AuNP-CC nanoparticles was examined using agar diffusion well method (Fig. 16). Two gram-negative bacteria: *Escherichia coli* and *Pseudomonas aeruginosa;* and two gram-positive bacteria: *Streptococcus mutans* and *Staphylococcus aureus* were used for the study. The high surface-to-volume ratio and smaller size of nanoparticles enable them to interact closely to the bacterial membrane

Table 4 Zone of inhibitions (mm) of CC extract, AuNP-CC and control against various bacteria

Bacterial cultures	CC extract (mm)	AuNP-CC (mm)	Distilled water (mm)
E. coli	0	13 ± 0.22	0
P. aeruginosa	11.2 ± 0.64	14.1 ± 0.42	0
S. aureus	0	12 ± 0.1	0
S. mutans	11.1 ± 0.4	12 ± 0.2	0

[46]. AuNP-CC penetrates into the cell wall and prevents the bacterial growth in the nearby region of the well due to its high affinity toward the phosphorus and sulfur containing biomolecules of the cell membrane [47]. This resulted in the membrane rupture and fatal to the pathogens. Table 2 provides the antibacterial efficiency of the nanoparticles measured in terms of the inhibition zone diameter (mm). The gram-negative bacteria showed maximum zone of inhibition on comparison with the gram-positive bacteria, due to the presence of very thin peptidoglycan layer present on its cell wall. The high thickness of peptidoglycan layers on the cell walls of gram-positive bacteria rather prevented the facile penetration of nanoparticles into the cytoplasmic membrane than gram-negative bacteria [48]. The higher zones of inhibition of AuNP-CC than CC extract prove its significant antibacterial activity (Table 4).

Conclusions

An effective and green microwave-assisted method was established for the synthesis of gold nanoparticles using the aqueous leaf extract of *Cyanthillium cinereum*. The methodology adopted was very simple, rapid and eco-friendly for the synthesis of gold nanoparticles. The *Cyanthillium cinereum* extract played an important role in the reduction and stabilization of the formed AuNP-CC nanoparticles through the electrostatic interactions provided by the respective phytoconstituents was evident from the FT-IR spectra. The synthesis of AuNP-CC was optimized and characterized. The crystalline face-centered cubic nature of the AuNP-CC was revealed from XRD and SAED studies. The various morphologies and particle size of 14.90 nm were determined from TEM. The DLS and zeta potential values provided evidences for their stability. The UV–vis. spectroscopy suggested that the formed nanoparticles as an excellent candidate for the catalytic reduction of o-/p-nitroanilines in aqueous media through $NaBH_4$ and fitted to the kinetics of pseudo-first order with good correlation coefficient. The linear dependence on rate of the reduction reaction with catalytic dosage was also explored during the study. AuNP-CC showed good anticancer properties against lung cancer cell line A549 than the CC extract. Hence, *Cyanthillium cinereum* stabilized gold nanoparticles can be effectively used as a powerful tool against cancer. AuNP-CC exhibited remarkable antibacterial activity against various human pathogenic bacteria. This work emphasized that the bio-fabricated noble metal nanoparticles as a cost effective and environment friendly alternative for the remediation of environmental pollutants.

Acknowledgements First author is grateful to University Grants Commission (UGC) for Senior Research Fellowship, and Department of Science & Technology (DST), Government of India for instrumentation facilities provided by DST-PURSE Phase II.

Data availability All data generated or analyzed during this study are included in this manuscript and its supplementary information files.

Declarations

Conflict of interest The authors declare that they have no conflict of interest.

Humans and animals statement The study does not involve the use of humans or animals.

Consent to participate All authors agree to participate in this investigation.

Consent for publication All authors agree to participate in this article.

References

1. Y. Mei, Y. Lu, F. Polzer, M. Ballauff, M. Drechsler, Chem. Mater. **19**, 1062 (2007)
2. X. Shi, K. Sun, J.R. Baker, J. Phy. Chem. C **112**, 8251 (2008)
3. R. Sardar, A.M. Funston, P. Mulvaney, R.W. Murray, Langmuir **25**, 13840 (2009)
4. H.H. Deng, G.W. Li, A.L. Liu, W. Chen, X.H. Lin, X.H. Xia, Microchim. Acta **181**, 911 (2014)
5. G.B. Reddy, D. Ramakrishna, A. Madhusudhan, D. Ayodhya, M. Venkatesham, G. Veerabhadram, J. Chin. Chem. Soc. **62**, 420 (2015)
6. A. Ulvestad, J.N. Clark, R. Harder, I.K. Robinson, O.G. Shpyrko, Nano Lett. **15**, 4066 (2015)
7. A.S.K. Hashmi, Chem. Rev. **107**, 3180 (2007)
8. K. Okitsu, M. Ashokkumar, F. Grieser, J. Phy. Chem. B **109**, 20673 (2005)
9. G. Sandmann, H. Dietz, W. Plieth, J. Electroanal. Chem. **491**, 78 (2000)
10. H. Sakai, T. Kanda, H. Shibata, T. Ohkubo, M. Abe, J. Am. Chem. Soc. **128**, 4944 (2006)
11. S. Sunkari, B.R. Gangapuram, R. Dadigala, R. Bandi, M. Alle, V. Guttena, J. Anal. Sci. Technol. **8**, 1 (2017)
12. G.B. Reddy, A. Madhusudhan, D. Ramakrishna, D. Ayodhya, M. Venkatesham, G. Veerabhadram, J. Nanostruct. Chem. **5**, 185 (2015)
13. M. Gholami-Shabani, M. Shams-Ghahfarokhi, Z. Gholami-Shabani, A. Akbarzadeh, G. Riazi, S. Ajdari, A. Amani, M. Razzaghi-Abyaneh, Process Biochem. **50**, 1076 (2015)
14. M.S. Punnoose, B. Mathew, Chem. Select **6**, 3584 (2021)
15. M.S. Punnoose, D. Bijimol, T. Abraham, N.J. Plathanam, B. Mathew, Bionanoscience **11**, 739 (2021)
16. A.G. Assefa, A.A. Mesfin, M.L. Akele, A.K. Alemu, B.R. Gangapuram, V. Guttena, M. Alle, J. Clust. Sci. **28**, 917 (2016)
17. S. Francis, S. Joseph, E.P. Koshy, B. Mathew, Environ. Sci. Pollut. Res. **24**, 17347 (2017)
18. R. Vijayan, S. Joseph, B. Mathew. IET Nanobiotechnol. **12**, 850 (2018)
19. R. Vijayan, S. Joseph, B. Mathew, Bionanoscience **8**, 105 (2018)
20. G. Guha, V. Rajkumar, R.A. Kumar, L. Mathew, Evid. Based Complement. Alternat. Med. **2011**, 1 (2011)
21. A. Chea, S. Hout, C. Long, L. Marcourt, R. Faure, N. Azas, R. Elias, Chem. Pharm. Bull. **54**, 1437 (2006)
22. C.J. Orendorff, T.K. Sau, C.J. Murphy, Small **2**, 636 (2006)
23. J. Fang, L. Yu, P. Gao, Y. Cai, Y. Wei, Anal. Biochem. **339**, 262 (2010)
24. C. Tiloke, A. Phulukdaree, K. Anand, R.M. Gengan, A.A. Chuturgoon, J. Cell Biochem. **117**, 2302 (2016)
25. S. Joseph, B. Mathew, J. Mol. Liq. **204**, 184 (2015)
26. M.S. Punnoose, D. Bijimol, B. Mathew, Enviro. Nanotechnol. Monit. Manag. **16**, 100525 (2021)

27. B. Zargar, H. Parham, A. Hatamie, Talanta **77**, 1328 (2009)
28. T.N.J.I. Edison, M.G. Sethuraman, Y.R. Lee, Res. Chem. Intermed. **42**, 713 (2015)
29. H.L. Lin, N.L. Sou, G.G. Huang, RSC Adv. **5**, 19248 (2015)
30. J. Huang, L. Zhang, B. Chen, N. Ji, F. Chen, Y. Zhang, Z. Zhang, Nanoscale **2**, 2733 (2010)
31. W. Wu, S. Liang, Y. Chen, L. Shen, H. Zheng, L. Wu, Catal. Commun. **17**, 39 (2012)
32. I.A. Wani, A. Ganguly, J. Ahmed, T. Ahmad, Mater. Lett. **65**, 520 (2011)
33. S.K. Ghosh, S. Kundu, M. Mandal, T. Pal, Langmuir **18**, 8756 (2002)
34. H.S. Lee, Y.W. Lin, Ann. Occup. Hyg. **53**, 289 (2009)
35. L. Kong, X. Lu, E. Jin, S. Jiang, X. Bian, W. Zhang, C. Wang, J. Solid State Chem. **182**, 2081 (2009)
36. T. Pal, S. De, N.R. Jana, N. Pradhan, R. Mandal, A. Pal, A.E. Beezer, J.C. Mitchell, Langmuir **14**, 4724 (1998)
37. N. Pradhan, A. Pal, T. Pa, Colloids Surf. A Physicochem. Eng. Asp. **196**, 247 (2002)
38. P. Dauthal, M. Mukhopadhyay *3 Biotech* **6**, 1 (2016)
39. S. Francis, E.P. Koshy, B. Mathew, Mater. Res. Express **5**, 045032 (2018)
40. R. Vijayan, S. Joseph, B. Mathew, Artif. Cells Nanomed. Biotechnol. **46**, 861 (2017)
41. S. Nag, A. Pramanik, D. Chattopadhyay, M. Bhattacharyya, Environ. Sci. Poll. Res. **25**, 2331 (2017)
42. V. Reddy, R.S. Torati, S. Oh, A. Kim, Ind. Eng. Chem. Res. **52**, 556 (2012)
43. C. Shi, N. Zhu, Y. Cao, P. Wu, Nanoscale Res. Lett. **10**, 1 (2015)
44. M.I. Din, R. Khalid, Z. Hussain, J. Najeeb, A. Sahrif, A.E. Intisar Ahmed, RSC Adv. **10**, 19041 (2020)
45. Y.K. Mohanta, S.K. Panda, R. Jayabalan, N. Sharma, A.K. Bastia, T.K. Mohanta, Front. Mol. Biosci. **4**, 14 (2017)
46. J.R. Morones, J.L. Elechiguerra, A. Camacho, K. Holt, J.B. Kouri, J.T. Ramírez, M.J. Yacaman, Nanotechnology **16**, 2346 (2005)
47. M.J. Hajipour, K.M. Fromm, A.A. Ashkarran, D.J. de Aberasturi, I.R. de Larramendi, T. Rojo, V. Serpooshan, W.J. Parak, M. Mahmoudi, Trends Biotechnol. **30**, 499 (2012)
48. M. Asariha, A. Chahardoli, N. Karimi, M. Gholamhosseinpour, A. Khoshroo, H. Nemati, Y. Shokoohinia, A. Fattahi, Bull. Mater. Sci. **43**, 1 (2020)

Authors and Affiliations

Mamatha Susan Punnoose[1] · Beena Mathew[1]

✉ Beena Mathew
beenamathew@mgu.ac.in

[1] School of Chemical Sciences, Mahatma Gandhi University, Kottayam, Kerala 686560, India